

Highly Floatable Superhydrophobic Metallic Assembly for Aquatic Applications

Zhibing Zhan, Mohamed ElKabbash, JinLuo Cheng, Jihua Zhang, Subhash Chandra Singh, and Chunlei Guo

ACS Appl. Mater. Interfaces, **Just Accepted Manuscript** • DOI: 10.1021/acsami.9b15540 • Publication Date (Web): 06 Nov 2019

Downloaded from pubs.acs.org on November 6, 2019

Just Accepted

“Just Accepted” manuscripts have been peer-reviewed and accepted for publication. They are posted online prior to technical editing, formatting for publication and author proofing. The American Chemical Society provides “Just Accepted” as a service to the research community to expedite the dissemination of scientific material as soon as possible after acceptance. “Just Accepted” manuscripts appear in full in PDF format accompanied by an HTML abstract. “Just Accepted” manuscripts have been fully peer reviewed, but should not be considered the official version of record. They are citable by the Digital Object Identifier (DOI®). “Just Accepted” is an optional service offered to authors. Therefore, the “Just Accepted” Web site may not include all articles that will be published in the journal. After a manuscript is technically edited and formatted, it will be removed from the “Just Accepted” Web site and published as an ASAP article. Note that technical editing may introduce minor changes to the manuscript text and/or graphics which could affect content, and all legal disclaimers and ethical guidelines that apply to the journal pertain. ACS cannot be held responsible for errors or consequences arising from the use of information contained in these “Just Accepted” manuscripts.

1
2
3
4
5
6
7
8
9
10
11
12
13
14
15
16
17
18
19
20
21
22
23
24
25
26
27
28
29
30
31
32
33
34
35
36
37
38
39
40
41
42
43
44
45
46
47
48
49
50
51
52
53
54
55
56
57
58
59
60

Highly Floatable Superhydrophobic Metallic Assembly for Aquatic Applications

*Zhibing Zhan^a, Mohamed ElKabbash^a, Jinluo Cheng^b, Jihua Zhang^a, Subhash Singh^{a,b}, Chunlei Guo^{*a,b}*

Email: guo@optics.rochester.edu

^a The Institute of Optics, University of Rochester, Rochester, New York 14627, USA

^b Changchun Institute of Optics, Fine Mechanics, and Physics, Changchun 130033, China

KEYWORDS: superhydrophobic surface, trapped air, femtosecond laser ablation, highly floatable assembly, aquatic application

1
2
3 ABSTRACT: Water-repellent superhydrophobic (SH) surfaces promise nearly endless
4 applications, from increased buoyancy to drag reduction, but their practical use is limited. This
5 comes from the fact that a SH surface will start to lose its efficiency once it is forced into water
6 or damaged by mechanical abrasion. Here, we circumvent these two most-challenging obstacles
7 and demonstrate a highly floating multi-faced SH metallic assembly inspired by the diving bell
8 spiders and fire ant assemblies. We study and optimize, both theoretically and experimentally,
9 the floating properties of the design. The assembly shows an unprecedented floating ability; it
10 can float back to surface even after being forced submerging under water for months. More
11 strikingly, the assembly maintains its floating ability even after severe damage and piercing in
12 stark contrast to conventional watercrafts and aquatic devices. The potential use of the SH
13 floating metallic assembly ranges from floating devices and electronic equipment protection, to
14 highly floatable ships and vessels.
15
16
17
18
19
20
21
22
23
24
25
26
27
28
29
30
31
32
33
34
35
36
37
38
39
40
41
42
43
44
45
46
47
48
49
50
51
52
53
54
55
56
57
58
59
60

Introduction

Water-repellent superhydrophobic (SH) surfaces promise nearly endless applications, from increased buoyancy to drag reduction¹⁻⁶, but their practical use is limited³. Typically, SH surfaces require extensive nano- and micro-scale surface textures and in most cases superhydrophobicity comes from a layer of air trapped among these structures^{5, 7-10}. This underlying mechanism imposes two fundamental hurdles that prevent SH surfaces from wide-spread use. First, once entirely submerged into water, SH surfaces will wet over time and relent its SH response¹¹⁻¹³. Second, the surface texture is susceptible to mechanical wear and abrasion, which can quickly degrade and eventually extinguish the surface superhydrophobicity^{1, 3, 14-15}. Here, we circumvent both these obstacles and demonstrate a highly floating multi-faced SH metallic assembly inspired by the diving bell (*Argyroneta aquatic*) spiders and fire ant assemblies that trap a large amount of air with their SH body surfaces even fully submerged under water without releasing the air cushion^[5]. We study, both theoretically and experimentally, the floating properties of the design. The assembly maintains its floating ability even after severe damage and piercing. We envision the applications of our highly floatable SH assemblies to range from replacing personal floating devices, to electronic equipment protection, and eventually large aquatic vessels to create super floatable boats or ships. Other materials can be processed to become SH and future research directions can include flexible materials to create floating, high loading capacity wearable devices and clothes that maintain their floating properties even after tearing or piercing.

Results and discussion

Argyroneta aquatic spiders live their entire lives underwater while maintaining a terrestrial respiratory system, *i.e.*, it breathes air¹⁶. The spiders create a dome-shaped web, so called diving

1
2
3 bell, between aquatic plants underwater and fill the diving bell with air carried from the water
4 surface by trapping air between their SH legs and abdomen and within the SH diving bell. The
5 ability of these creatures to sustain the SH functionality indicates that they evolved to maintain
6 their superhydrophobicity even after being fully submerged in water indefinitely. Furthermore, fire
7 ants can self-assemble and form a raft by trapping a large volume of air among their SH bodies¹⁷.
8 The key insight is that multifaced SH surfaces can trap a large air volume which points towards
9 the possibility of using SH surfaces to create buoyant devices for aquatic applications. Inspired by
10 these two species, we present a design of a highly floating device. We note that a single SH metal
11 can float on water surface^{4, 18-19}; however, if a force is exerted downward exceeding the loading
12 capacity, the SH metal will permanently sink and relent its SH properties, *i.e.*, even after it is
13 brought back to the surface it may not float (Figure 1a and Movie S1 in Supplementary Materials).
14 Our assembly consists of two parallel Aluminum (Al) plates that are treated to become SH and
15 connected by a plastic post (Figure 1b and Figure S1). The two SH surfaces face each other so that
16 they are enclosed and free from external wear and abrasion, while the outer surfaces are regular
17 untreated Al. Because of the water repellency of the SH surfaces, this assembly will trap a large
18 volume of air under water and the assembly will float back to the surface even forced into water
19 (Figure 1e, and Movie S1). Figure 1d shows a SH assembly forced submerged under water by a
20 load traps an air bubble between the metal plates (Figure 1d-inset). After the load is released, the
21 SH assembly floats back to the surface (Figure 1e and Movie S2). On the other hand, the same
22 assembly consisting of two untreated Al disks remains sunk and no air is trapped between the disks
23 (see Figures 1d, S1 and Movie S3).
24
25
26
27
28
29
30
31
32
33
34
35
36
37
38
39
40
41
42
43
44
45
46
47
48
49
50
51
52
53
54
55
56
57
58
59
60

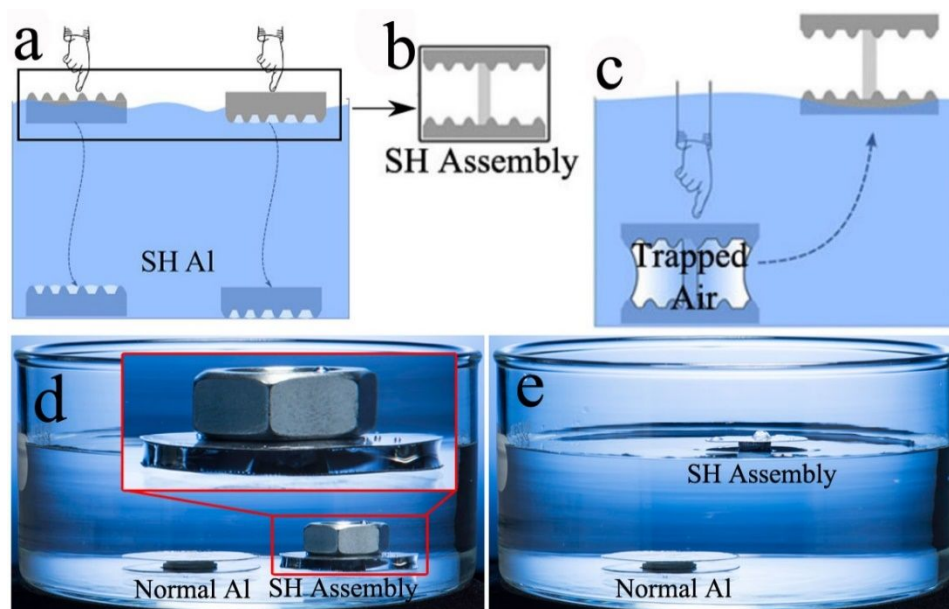


Figure 1. Design principle of the highly floatable superhydrophobic metallic assembly. (a-c) Schematics show two SH Al disks (a) sink to the bottom of the beaker after piercing the water surface. (b) Design of the SH assembly which consists of two Al disks such that their inner surfaces are treated to be SH. The Al disks are connected by a plastic post. (c) A SH assembly forced to sink under water will float back to the surface when the load is released. (d) An image of the assembly forced to sink due to a heavy load while trapping an air bubble between the SH Al disks. The same assembly with bare Al, however, is unable to float. (e) An image showing the SH assembly floating back to the surface after the load is released.

A surface is considered SH if a water droplet beads up on the surface with a contact angle (CA) $\theta > 150^\circ$ ^{2, 20-23}. To create a SH Al surface, we use a direct femtosecond (fs) laser processing technique to produce a range of hierarchical micro- and nano-structures on Al. Fs laser technique can directly create micro/nanoscale hierarchical structures on a wide variety of materials by a simple one-step scanning method²⁴⁻²⁶, which is a powerful method for research of various special

1
2
3 surface wetting properties ^{7, 14-15, 20, 22, 27-32}. To further control the degree of hydrophobicity, we
4
5 control the surface morphology by varying the laser processing conditions and the surface energy
6
7 by immersing the structured Al surface in aqueous ethanol solution of stearic acid for various
8
9 durations. Details on the experimental setup and fabrication processes are described in
10
11 supplementary materials (Methods section). Without fs laser treatment, CA for bare Al is only
12
13 $\sim 54^\circ$ see Figure 2a and 2b. Similar to our previous work ^{15, 27}, fs laser processing also turns the
14
15 treated area pitch black with the near-unity optical absorption (Figure 2c) ^{15, 27}. As shown in Figure
16
17 2d, Al becomes black and SH with $\theta \sim 168^\circ$ following fs laser and chemical treatments. Figure 2e
18
19 and 2f shows SEM images of typical hierarchical micro- and nano-structures formed on the Al
20
21 surface following fs laser treatment. The structure consists of an array of microgrooves (Figure 2e)
22
23 covered by extensive nanostructures (Figure 2f), also see Figure S2 for more SEM images. The
24
25 surface morphology is also measured using confocal UV laser microscope shown in Figure 2g and
26
27 2h. The strong water repellency of our SH Al is captured by water droplet bouncing from the
28
29 surface shown in Figure 2i and Movie S4.
30
31
32
33
34
35
36
37
38
39
40
41
42
43
44
45
46
47
48
49
50
51
52
53
54
55
56
57
58
59
60

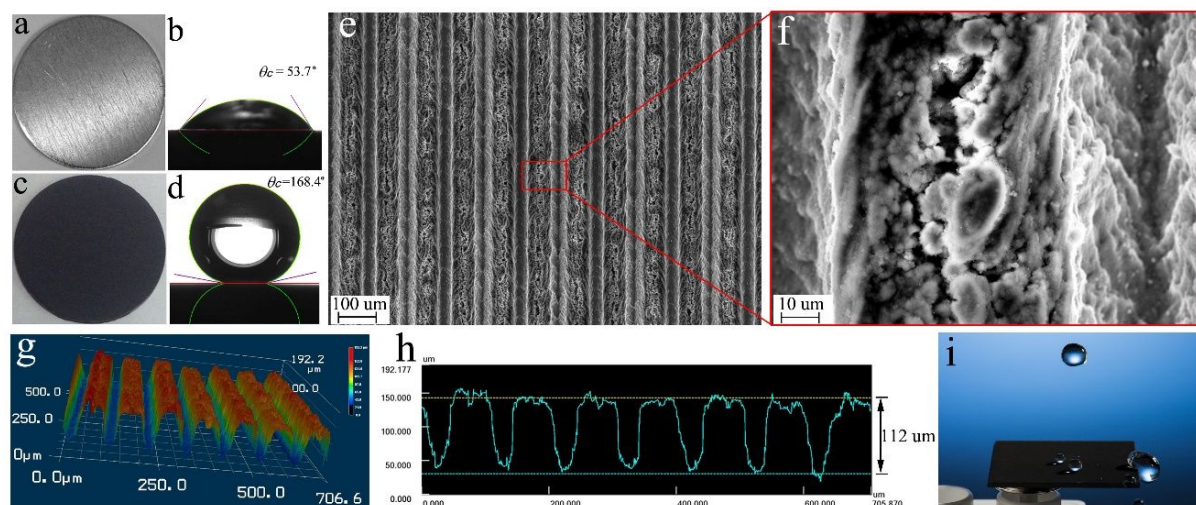


Figure 2. Femtosecond laser treated SH Al surface. (a-d) Sample photos and corresponding water CA of a bare Al surface (a and b), and that with fs laser treatment and stearic acid modification (c and d). (e and f) SEM images of Al surfaces after fs laser treatment. (g and h) Confocal UV laser microscope image of the three-dimensional surface profile (g) and a cross section showing the height variation (h). (i) Photo of water droplets bouncing off the fs laser treated SH surface.

The gap distance between the two Al plates, H , is a key parameter in our design. There is a minimum H value for the assembly to trap enough air to keep itself floated (H_{\min}) (see Figure 3a). A larger H will trap more air and increase the buoyancy and loading capacity of the device, however, there exists a maximum H where the assembly lose its buoyancy as it can no longer trap air inside (H_{\max}). Therefore, our first study is to determine the admissible range of H for the assembly to stay afloat. H_{\min} is determined by equating the weight of the overall assembly to the displaced water. Using our assembly with the Al disk thickness of 0.2 mm, H_{\min} is ~ 0.68 mm (see Supplementary Information). This value agrees with our experimentally observed value of 0.761 mm (Figure S3), where the assembly will remain stationary, neither rise nor sink (Figure 3b). The

discrepancy between calculated and demonstrated H_{min} is due to the approximation in the calculations and the additional weight of the plastic post and glue used for preparing the assembly (Figure S1). Note that H_{min} is independent of the Al disk radius (R).

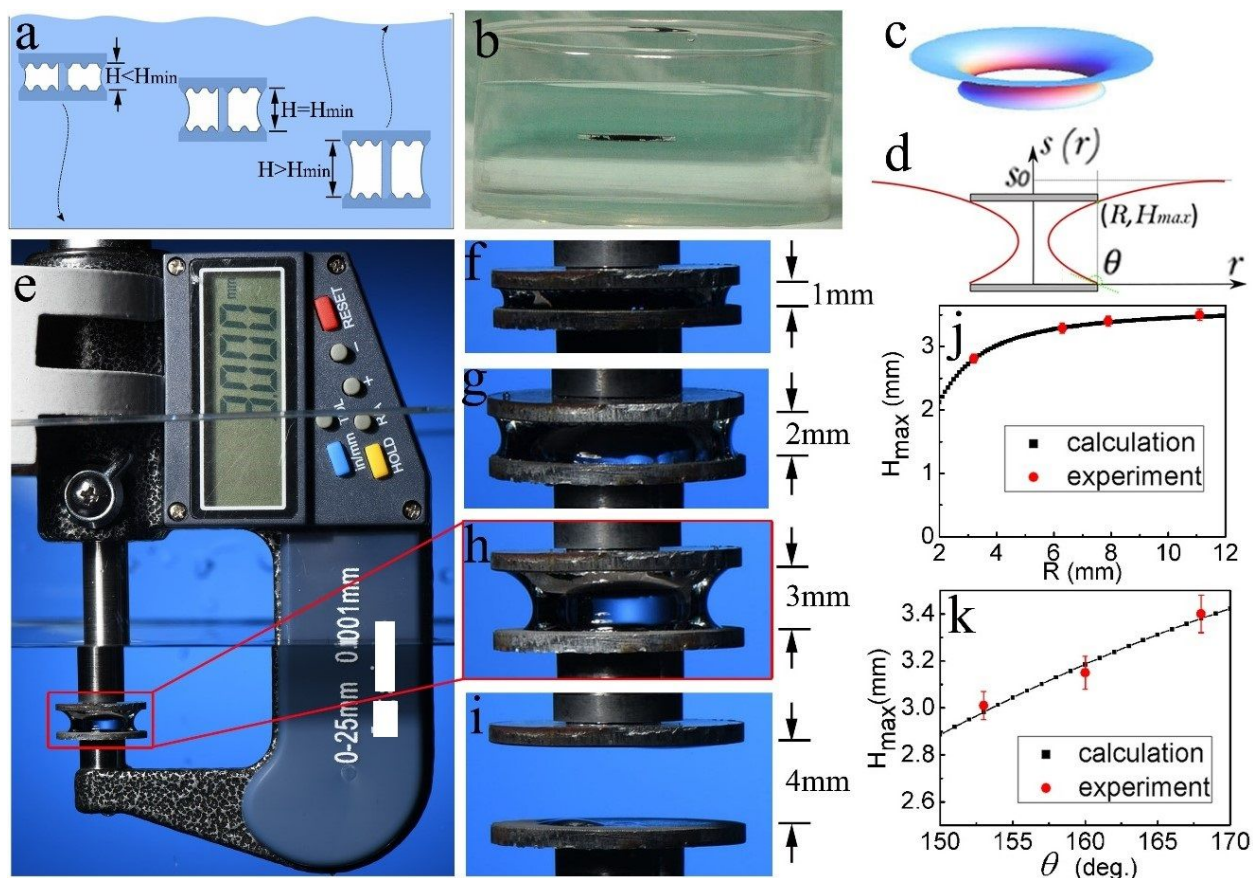


Figure 3. Design parameters: Determination of the gap distance range of multifaced SH assembly. (a) Schematic of the gap distance (H) effect on the assembly buoyancy. (b) An image of the assembly with $H = H_{min}$ staying stationary in water. (c and d) Calculated topography of the dimple formed on water surface after placing a single SH surface (c) and a schematic illustrating the dependence of H_{max} on R and θ (d). (e) Photo of the experimental setup used to determine H_{max} . (f-i) Photos of the trapped air underwater with $H = 1.0$ mm (f), $H = 2.0$ mm (g), $H = 3.0$ mm (h), and $H = 4.0$ mm (i). (j and k) Experimental and calculated results of the largest gap distance (H_{max}) as a function of the SH surface radius (j) and CA (k).

Next, we investigate the maximum possible gap distance, H_{\max} , as a function of the Al disk radius and surface hydrophobicity. To find H_{\max} theoretically, our approach is to consider a single SH plate with radius R floating on the water surface. The water surface will form a dimple and the dimple topography $s(x, y)$, at equilibrium, is determined by the Young-Laplace equation, $\rho_W g s = \sigma \nabla \cdot \hat{n}$, where ρ_W is the water density, σ is the water-air interfacial energy, g is the gravity constant, $s = s(x, y)$ is the formed dimple surface, and $\hat{n} = \hat{n}(x, y)$ is the surface normal vector^{19, 33-35}. In our system, the Young-Laplace equation can be expressed in polar coordinate as following

$$\frac{\rho_W g}{\sigma} (s - s_0) = \frac{1}{r} \frac{d}{dr} \frac{rs'(r)}{\sqrt{1 + [s'(r)]^2}} \quad (1)$$

where $s_0 = s(\infty)$ is the dimple height from the water surface at infinity, *i.e.*, approaching the waterline where the dimple vanishes. By setting $\xi = \rho_W g / \sigma$ and $s'(r) = \tan \varphi$ with $\varphi \in (0, \theta]$ (θ is the CA), the above equation can be converted to the parameter space as

$$\frac{dr(\varphi)}{d\varphi} = \frac{r(\varphi) \cos \varphi}{\xi r(\varphi) [s_0 - s(\varphi)] + \sin \varphi} \quad (2)$$

$$\frac{ds(\varphi)}{d\varphi} = \tan \varphi \frac{dr(\varphi)}{d\varphi} \quad (3)$$

$$r(\theta_c) = R, s(\theta_c) = 0 \quad (4)$$

For a given s_0 , the above differential equations can be solved numerically. The real solution is obtained when the given s_0 satisfies $s_0 = s(\varphi = 0)$. When the top Al plate has the same radius as the bottom plate, the maximum gap distance that enables air trapping is $H_{\max} = s(\varphi_0)$ on the surface with φ_0 different from θ and satisfying $r(\varphi_0) = R$. The calculated 3D dimple topography is shown in Figure 3c, and the dependence of H_{\max} on the diameters and on the CAs of the SH Al

1
2
3 surfaces are shown in Figure 3J and 3K (all data can be found in supporting information Table
4 S1). The calculational details are presented in the supporting information.
5
6
7

8 To determine experimentally H_{\max} , we use a high-resolution digital micrometer and attach
9 two aligned Al SH surfaces to the micrometer legs. First, we have the two surfaces touching each
10 other and reset the digital micrometer to zero (see Figure S4). Next, we increase the gap distance
11 outside of water, set it to a certain value, and adiabatically immerse the assembly to ~ 1 cm (see
12 Figure 3e) below the water surface. The adiabatic process here means that the SH assembly is
13 immersed into the water rapid enough that the trapped air does not leak out. The beaker is filled
14 with water to ~ 5 cm high, and the water pressure variation over the 5 cm is $\sim 0.5\%$ of atmospheric
15 pressure so that the effect of the water depth is negligible. Since our study focuses on floating
16 effect and the SH assembly always floats back to surface after being forced into water, we neglect
17 deep-water pressure effect and leave it for future investigations. For small H , here 1 mm, the
18 trapped air bubble takes an approximate shape of a cylinder close to the diameter of the disk
19 (Figure 3f). When H increases to 2 mm and 3 mm, the trapped air takes a clearer form of a
20 hyperboloid (Figure 3g and 3h). Finally, at $H = 4$ mm, the SH plates are incapable of trapping air
21 (Figure 3i). To study the dependence of H_{\max} on the disk radius R and the water-solid CA, we
22 fabricate a series of samples with $R = 3.2, 6.3, 7.9$ and 11.1 mm with $\theta = 168^\circ$ (Figure S5) and CA
23 $\theta \sim 153^\circ, 160^\circ$, and 168° with $R = 7.9$ mm (Figure S6). Figure 3j shows the experimental and
24 calculated results for H_{\max} as a function of R (two examples are shown in Figure S7). For smaller
25 R values, H_{\max} increases with R while for larger R values, H_{\max} becomes a constant. Figure 3k
26 shows the experimental and calculated results for H_{\max} as a function of CA. As expected, a larger
27 CA (stronger hydrophobicity) results in a larger H_{\max} .
28
29
30
31
32
33
34
35
36
37
38
39
40
41
42
43
44
45
46
47
48
49
50
51
52
53
54
55
56
57
58
59
60

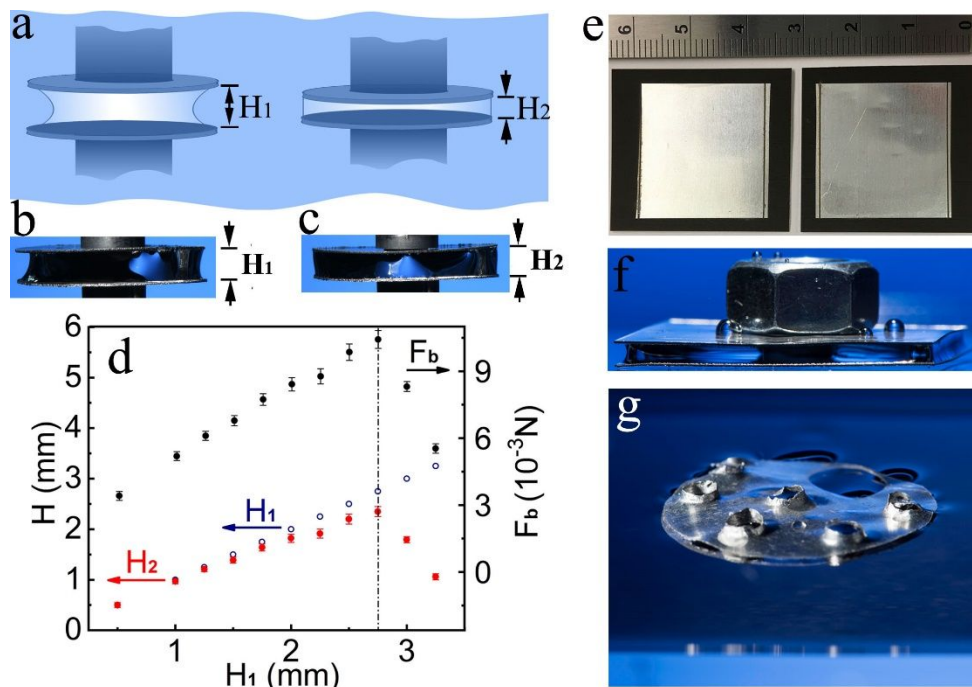


Figure 4. Applications: loading capacity and durability after severe damage. (a) Schematic of the gap distances H_1 and H_2 : we started with an initial gap distance H_1 , then reduced the gap distance underwater to minimize the gap so that the trapped air will take the form of an ideal cylinder that has radius R and gap distance H_2 . (b and c) Photos of the trapped air topology in water for an initial gap distance (H_1) (here, 2.75 mm) (b), and the gap distance where the trapped air takes the form of a regular cylinder in water (H_2) (here, 2.338 mm) (c). (d) The dependence of H_2 on H_1 , and the corresponding buoyancy force (F_b) based on H_2 . (e) Two Al squares with area ~ 30 mm \times 30 mm with only ~ 3 mm width frame treated with fs laser to be SH (black frame). (f) SH assembly based on the Al squares shown in (e) submerged under water with a heavy load while trapping an air bubble. (g) A SH assembly remains floating even after significant structural damage (six smaller through holes each with a 3-mm diameter and one larger through hole with a 6-mm diameter).

Experimentally, as we submerge the assembly adiabatically into the water, there will be air loss during the submersion process and this air loss is more pronounced with a larger initial gap

1
2
3 distance. Therefore, the diameter of the trapped air column decreases with gap distance H , as
4 shown in Figure 3. Accordingly, it is difficult to quantitatively estimate the volume of the trapped
5 air only by knowing H . For example, it is difficult to tell if the volume of the entrapped air in
6 Figure 3h is greater than that in Figure 3g, although Figure 3h has a larger H . To determine the H
7 value that gives the maximum buoyancy force F_b , we started with an initial gap distance H_1 , then
8 reduced the gap distance underwater to minimize the curvature so that the trapped air takes the
9 form of an ideal cylinder that has a radius R and a gap distance H_2 (see schematic Figure 4a).
10 Example images of the trapped air column with $H_1 = 2.75$ and $H_2 = 2.338$ mm are shown in Figure
11 4b and 4c, respectively, for an assembly of $R = 11.1$ mm and $\theta = 168^\circ$ (see Figure S8). For a given
12 H_1 , the trapped air volume and the corresponding buoyancy force F_b can be readily calculated
13 using H_2 according to the following equation: $F_b = \rho_W g \pi R^2 (H_2 + 2h_M)$, where R and h_M are radius
14 and thickness of our Al SH plates (11.1 and 0.2 mm in this case), respectively. The calculated
15 results for F_b are shown in Figure 4d (black round). The linear change of H vs. H_1 is also plotted
16 in Figure 4d. For SH Al disks of $R = 11.1$ mm, when $H_1 < 2.75$ mm, H_2 increases with H_1 , which
17 means that by simply increasing the gap distance, the trapped air volume, and buoyancy, increases.
18 For $H_1 > 2.75$ mm, H_2 decreases with H_1 , due to the decrease in the trapped air radius that we noted
19 earlier in comparing Figure 3g and 3h. In the demonstrated case, the largest buoyancy force for
20 the SH Al assembly corresponds to $H_1 \sim 2.75$ mm. Therefore, we prepared an assembly with $H =$
21 2.75 mm and $R = 11.1$ mm, and tested its loading capacity. The assembly can float back to the
22 water surface even with a load of 2.5 times of its weight (Movie S5 and Figure S9). The maximum
23 loading capacity (1.021 g here) agrees well with the calculated maximum buoyancy shown in
24 Figure 4d ($F_b = 0.01043$ N, which corresponds to 1.064 g). If the intended application is to create
25 a floating device with high loading capacity, we note that it is sufficient to only transform the outer
26
27
28
29
30
31
32
33
34
35
36
37
38
39
40
41
42
43
44
45
46
47
48
49
50
51
52
53
54
55
56
57
58
59
60

1
2
3 rim of the metal plates to be SH instead of the entire plates, as shown in Figure 4e. Indeed, the
4 device will trap an air bubble and remain afloat after releasing load as shown in Figure 4f and
5 Movie S6. For an assembly with a given H , the loading capacity scales with R^2 , for example for H
6 = 2.75 mm, an assembly with $R = 13.82$ m can handle a load of 1 ton, while the required area
7 treated to be SH is only about 0.5 m² (see Figures S10 and S11).
8
9

10
11
12
13
14
15 Although the SH surface textures are susceptible to mechanical wear and tear, our design
16 overcomes this problem since the SH surfaces are enclosed within the assembly and they are
17 neither in direct contact with any external load nor the water. For a durability test, a loaded SH
18 assembly has been left in water for two months, and the assembly remains floating for the entire
19 period without sinking or any observed deterioration. We note that the trapped air remains
20 under water due to loading for the entire period (see Figure S9). Another important advantage of
21 the SH assembly is that although the floating principle is the same as other floating device, *e.g.*
22 ships, the assembly structure can withstand severe damage and even substantial piercing without
23 sinking. If the air entrapment was due to conventional methods of concealment, water will rush
24 inside the device after piercing, *e.g.* damaging a ship's hull or piercing a personal floating device,
25 and it will sink if the floating object is denser than water. However, in our design, the SH assembly
26 automatically conceals the entrapped air even if the SH metals are pierced and water replaces the
27 trapped air within the pierced volume (Figure 4g). In principle, no matter how many holes are
28 drilled through the assembly, the structure will float because the water volume is replaced by water
29 so the buoyancy condition of the entire structure is still satisfied (schematics shown in Figure S12).
30 Figure 4g shows a severely pierced SH assembly (~20% of the structure is removed) without
31 affecting its ability to float (see Movie S7). More clearer images show the severely pierced SH
32 assembly on water surface can be found in Figure S13. No water rushes inside the assembly, which
33
34
35
36
37
38
39
40
41
42
43
44
45
46
47
48
49
50
51
52
53
54
55
56
57
58
59
60

1
2
3 is in stark contrast to conventional buoyant devices comprised of denser-than-water materials.
4
5 Furthermore, the severely pierced SH assembly can float back to the water surface very quickly
6
7 (about 2.5 second) even after being immersed in a deep (44 cm) container, as shown in Movie S8.
8
9 Note, a watercraft or a personal floating device made of denser-than-water material(s) would sink
10
11 if pierced. On the other hand, the existence of two SH plates conceals the trapped air automatically
12
13 after piercing and no water can rush inside the plates, which is a unique property for our assembly.
14
15
16

17 **Conclusion**

18
19
20
21 This work demonstrated how to use SH effects to render metals highly floatable. Our design
22
23 overcame the most fundamental hurdles preventing SH surfaces from practical applications,
24
25 namely, wetting the SH surface after being submerged into water and mechanical wear and tear.
26
27 The work serves as a starting point to develop biomimetic designs inspired by creatures utilizing
28
29 their SH surfaces even fully submerged under water. The ability of the SH assemblies to remain
30
31 afloat after severe structural damage is unique compared to conventional floating devices and
32
33 watercrafts that have been used for millennia. Using a stack of SH assembly can further increase
34
35 the loading capacity per unit surface area, which is more suitable for constructing large aquatic
36
37 vessels. The applications of the highly floatable SH assembly can range from constructing personal
38
39 floating devices, electronic equipment protection, to floatable boats or ships. For example,
40
41 inflatable floating devices cannot float after piercing, which can be overcome using our design
42
43 concept. As other materials can be processed to become SH, future research can investigate flexible
44
45 materials to create floating and high loading capacity wearable devices that can survive tearing
46
47 and piercing.
48
49
50
51
52
53
54
55
56
57
58
59
60

Experimental Section

Aluminum plates with thickness of 0.2 and 1.0 mm with purity of 99.9% were purchased from GoodFellow, and degreased in acetone before laser ablation. Stearic acid (98%) and absolute ethanol were purchased from Alfa Aesar. All chemicals were analytical grade reagents and were used as received.

The Al was first processed by femtosecond (fs) laser pulses to obtain hierarchical micro- and nano-scale surface structures, as shown in Figure S14. In our experiments, an amplified Ti:sapphire laser system was used that generates 65-fs pulses with a central wavelength of 800 nm and at a maximum pulse repetition rate of 1 kHz. The laser beam was focused onto the sample surface mounted on a computerized XY-translation stage. The pulse energy from the fs laser was about 0.8 mJ, and the linear velocity of the translation stage is 1 mm/s. To control the superhydrophobicity, we also use pulse energy of 0.4 and 0.2 mJ. The period between the adjacent scanning lines is 100 μm . To further control the degree of hydrophobicity, we control the surface morphology by varying the laser processing conditions and the surface energy through immersing the structured Al surface in aqueous ethanol solution of stearic acid (0.01M) for various durations. Afterwards, the sample was rinsed by pure ethanol and dried in 60 °C oven for 30 min.

Water droplet with a diameter of about 2.8 mm was generated from a syringe tip that was connected to a syringe pump. Water droplets were dropped from a height of 80 mm (tip to surface). The spreading and retraction dynamics of the droplet on the surfaces were recorded using a high-speed camera (NAC, HotShot 1280 cc) with 3000 frames per second.

SH assemblies were prepared by using plastic rings with different heights to control the gap distances between two SH Al plates, as shown in Figure S1. The plastic rings were first cut from a plastic tube with outside diameter of about 7.0 mm and tube thickness of 0.9 mm. The rings

1
2
3 were then abraded by sandpapers to obtain the desired height in order to control the gap distance
4
5 in SH assembly. An epoxy (Loctite EA 450 A&B) was used to glue the plastic post to the two
6
7 aligned SH Al plates to form an Al SH assembly. The two SH Al surfaces face each other so that
8
9 they are enclosed and free from external wear and abrasion, while the outer surfaces can be
10
11 regular untreated Al. Finally, the SH assembly was placed in an oven with temperature of 50 °C
12
13 for 60 min to dry totally. The additional load test was carried out by sticking an Al plate with the
14
15 radius 11.1 mm and thickness 1.0 mm on the bottom of the assembly to avoid the overturning of
16
17 the sample when it is floating to water surface. To test the piercing effect, the SH assembly was
18
19 purposely damaged by drilling several holes on through the SH assembly.
20
21
22
23

24 The surface structures were first analyzed by a confocal UV scanning laser microscope
25
26 (KEYENCE, VK-9700) that resolves microstructures and provides a larger viewing area. For a
27
28 more detailed view, a Scanning Electron Microscopy (SEM) was used to determine micro- and
29
30 nano-scale surfaces down to 10 nm resolution. The SEM is a Zeiss- Auriga Field Emission SEM
31
32 operating at an accelerating voltage of 20 kV. The surface CA were measured by Kino SL200KB
33
34 Contact Angle Meter.
35
36
37
38
39

40 ASSOCIATED CONTENT

41
42
43 **Supporting Information:** Photos of normal and SH assemblies, SEM images of the SH Al
44
45 surface, photos of the SH assembly with H_{min} and the digital micrometer used in this work, SH
46
47 surfaces with different diameters, SEM images and photos of SH surfaces with different contact
48
49 angles, photos of the samples to determine H_{max} and F_b , loading test of the SH assembly,
50
51 schematics of the loading capacity and treated areas of the SH assembly, schematics of the air
52
53 volume of a severely pierced SH assembly and its photos, and experimental setup for fs laser
54
55
56
57
58
59
60

1
2
3 processing; detailed calculation processes of the H_{min} and H_{max} ; and additional movies show the
4 SH Al surface, SH assembly, and floating properties of the assemblies. This material is available
5
6 free of charge via the Internet at <http://pubs.acs.org>.
7
8
9
10
11
12
13
14
15
16

17 AUTHOR INFORMATION

18 19 **Corresponding Author**

20
21 guo@optics.rochester.edu
22
23
24

25 ACKNOWLEDGMENT

26
27
28 This work was supported by the Bill & Melinda Gates Foundation (OPP1157723), the US Army
29 Research Office (W911NF-15-1-0319), and National Science Foundation (1701163 & 1722169)
30 grants. The authors would like to acknowledge A. Fenster and M. Mann for their assistance in
31 recording high-quality photos and videos, and J.-H. Kim and J. Shang for their assistance in
32 recording water bouncing videos.
33
34
35
36
37
38
39

40 REFERENCES

- 41
42 1. Lu, Y.; Sathasivam, S.; Song, J. L.; Crick, C. R.; Carmalt, C. J.; Parkin, I. P., Robust
43 Self-Cleaning Surfaces that Function when Exposed to either Air or Oil. *Science* **2015**, *347*,
44 1132-1135.
- 45 2. Liu, T. Y.; Kim, C. J., Turning a Surface Superrepellent Even to Completely Wetting
46 Liquids. *Science* **2014**, *346*, 1096-1100.
- 47 3. Tian, X. L.; Verho, T.; Ras, R. H. A., Moving Superhydrophobic Surfaces Toward Real-
48 World Applications. *Science* **2016**, *352*, 142-143.
- 49 4. Pan, Q. M.; Wang, M., Miniature Boats with Striking Loading Capacity Fabricated from
50 Superhydrophobic Copper Meshes. *ACS Appl. Mater. Interfaces* **2009**, *1*, 420-423.
- 51 5. Tiginyanu, I.; Braniste, T.; Smazna, D.; Deng, M.; Schutt, F.; Schuchardt, A.; Stevens-
52 Kalceff, M. A.; Raevschi, S.; Schurmann, U.; Kienle, L.; Pugno, N. M.; Mishra, Y. K.; Adelung,
53
54
55
56
57
58
59
60

- R., Self-Organized and Self-Propelled Aero-GaN with Dual Hydrophilic-Hydrophobic Behaviour. *Nano Energy* **2019**, *56*, 759-769.
6. Nystrom, G.; Fernandez-Ronco, M. P.; Bolisetty, S.; Mazzotti, M.; Mezzenga, R., Amyloid Templated Gold Aerogels. *Adv. Mater.* **2016**, *28*, 472-478.
7. Yong, J. L.; Singh, S. C.; Zhan, Z. B.; Chen, F.; Guo, C. L., Substrate-Independent, Fast, and Reversible Switching between Underwater Superaerophobicity and Aerophilicity on the Femtosecond Laser-Induced Superhydrophobic Surfaces for Selectively Repelling or Capturing Bubbles in Water. *ACS Appl. Mater. Interfaces* **2019**, *11*, 8667-8675.
8. Gao, X. F.; Jiang, L., Water-Repellent Legs of Water Striders. *Nature* **2004**, *432*, 36-36.
9. Peaudecerf, F. J.; Landel, J. R.; Goldstein, R. E.; Luzzatto-Fegiz, P., Traces of Surfactants Can Severely Limit the Drag Reduction of Superhydrophobic Surfaces. *Proc. Natl. Acad. Sci. U. S. A.* **2017**, *114*, 7254-7259.
10. Zhan, Z. B.; Li, Z. H.; Yu, Z.; Singh, S.; Guo, C. L., Superhydrophobic Al Surfaces with Properties of Anticorrosion and Reparability. *ACS Omega* **2018**, *3*, 17425-17429.
11. Lee, C.; Kim, C. J., Underwater Restoration and Retention of Gases on Superhydrophobic Surfaces for Drag Reduction. *Phys. Rev. Lett.* **2011**, *106*, 014502
12. Lv, P. Y.; Xue, Y. H.; Shi, Y. P.; Lin, H.; Duan, H. L., Metastable States and Wetting Transition of Submerged Superhydrophobic Structures. *Phys. Rev. Lett.* **2014**, *112*, 196101.
13. Hof, B., Water Flows out of Touch. *Nature* **2017**, *541*, 161-162.
14. Zhan, Z. B.; Garcell, E. M.; Guo, C. L., Robust Mold Fabricated by Femtosecond Laser Pulses for Continuous Thermal Imprinting of Superhydrophobic Surfaces. *Mater. Res. Express* **2019**, *6*, 075011.
15. Zhan, Z. B.; Li, Z. H.; Li, X. Y.; Garcell, E.; Singh, S.; ElKabbash, M.; Guo, C. L., Creating Superhydrophobic Polymer Surfaces with Superstrong Resistance to Harsh Cleaning and Mechanical Abrasion Fabricated by Scalable One-Step Thermal-Imprinting. *Adv. Mater. Interfaces* **2019**, *6*, 1900240.
16. Mlot, N. J.; Tovey, C. A.; Hu, D. L., Fire Ants Self-Assemble into Waterproof Rafts to Survive Floods. *Proc. Natl. Acad. Sci. U. S. A.* **2011**, *108*, 7669-7673.
17. Seymour, R. S.; Hetz, S. K., The Diving Bell and the Spider: the Physical Gill of *Argyroneta Aquatica*. *J. Exp. Biol.* **2011**, *214*, 2175-2181.
18. Yong, J. L.; Yang, Q.; Chen, F.; Zhang, D. S.; Du, G. Q.; Si, J. H.; Yun, F.; Hou, X., A Bioinspired Planar Superhydrophobic Microboat. *J. Micromech. Microeng.* **2014**, *24*, 035006.
19. Pan, Q. M.; Liu, J.; Zhu, Q., A Water Strider-Like Model with Large and Stable Loading Capacity Fabricated from Superhydrophobic Copper Foils. *ACS Appl. Mater. Interfaces* **2010**, *2*, 2026-2030.
20. Yong, J. L.; Zhan, Z. B.; Singh, S. C.; Chen, F.; Guo, C. L., Femtosecond Laser-Structured Underwater "Superpolymphobic" Surfaces. *Langmuir* **2019**, *35*, 9318-9322.
21. Feng, L.; Li, S. H.; Li, Y. S.; Li, H. J.; Zhang, L. J.; Zhai, J.; Song, Y. L.; Liu, B. Q.; Jiang, L.; Zhu, D. B., Super-Hydrophobic Surfaces: From Natural to Artificial. *Adv. Mater.* **2002**, *14*, 1857-1860.
22. Chu, D. K.; Singh, S. C.; Yong, J. L.; Zhan, Z. B.; Sun, X. Y.; Duan, J. A.; Guo, C. L., Superamphiphobic Surfaces with Controllable Adhesion Fabricated by Femtosecond Laser Bessel Beam on PTFE. *Adv. Mater. Interfaces* **2019**, *6*, 1900550.
23. Sun, T. L.; Wang, G. J.; Feng, L.; Liu, B. Q.; Ma, Y. M.; Jiang, L.; Zhu, D. B., Reversible Switching between Superhydrophilicity and Superhydrophobicity. *Angew. Chem.-Int. Edit.* **2004**, *43*, 357-360.

- 1
2
3 24. Kietzig, A. M.; Hatzikiriakos, S. G.; Englezos, P., Patterned Superhydrophobic Metallic
4 Surfaces. *Langmuir* **2009**, *25*, 4821-4827.
- 5 25. Kietzig, A. M.; Mirvakili, M. N.; Kamal, S.; Englezos, P.; Hatzikiriakos, S. G., Laser-
6 Patterned Super-Hydrophobic Pure Metallic Substrates: Cassie to Wenzel Wetting Transitions. *J.*
7 *Adhes. Sci. Technol.* **2011**, *25*, 2789-2809.
- 8 26. Kietzig, A. M.; Mirvakilia, M. N.; Kamalb, S.; Englezosa, P.; Hatzikiriakosa, S. G.,
9 Nanopatterned Metallic Surfaces: Their Wettability and Impact on Ice Friction. *J. Adhes. Sci.*
10 *Technol.* **2011**, *25*, 1293-1303.
- 11 27. Vorobyev, A. Y.; Guo, C. L., Multifunctional Surfaces Produced by Femtosecond Laser
12 Pulses. *J. Appl. Phys.* **2015**, *117*, 033103.
- 13 28. Chu, D. K.; Singh, S. C.; Zhan, Z. B.; Su, X. Y.; Duan, J. A.; Guo, C. L., Creation of
14 Enhanced Transmission for Clear and Frosted Glass through Facile Surface Texturing. *Opt.*
15 *Mater. Express* **2019**, *9*, 2946-2954.
- 16 29. He, Y. Z.; Zhang, J. H.; Singh, S.; Garcell, E.; Vorobyev, A. Y.; Lam, B.; Zhan, Z. B.;
17 Yang, J. J.; Guo, C. L., Maskless Laser Nano-Lithography of Glass through Sequential
18 Activation of Multi-Threshold Ablation. *Appl. Phys. Lett.* **2019**, *114*, 133107.
- 19 30. Lu, J. L.; Yang, J. J.; Singh, S. C.; Zhan, Z. B.; Yu, Z.; Xin, W.; Huang, T.; Guo, C. L.,
20 Hierarchical Micro/nanostructured TiO₂/Ag Substrates Based on Femtosecond Laser Structuring:
21 A Facile Route for Enhanced SERS Performance and Location Predictability. *Appl. Surf. Sci.*
22 **2019**, *478*, 737-743.
- 23 31. Yong, J. L.; Singh, S. C.; Zhan, Z. B.; Chen, F.; Guo, C. L., How To Obtain Six Different
24 Superwettabilities on a Same Microstructured Pattern: Relationship between Various
25 Superwettabilities in Different Solid/Liquid/Gas Systems. *Langmuir* **2019**, *35*, 921-927.
- 26 32. Yong, J. L.; Singh, S. C.; Zhan, Z. B.; Huo, J. L.; Chen, F.; Guo, C. L., Reducing
27 Adhesion for Dispensing Tiny Water/Oil Droplets and Gas Bubbles by Femtosecond Laser-
28 Treated Needle Nozzles: Superhydrophobicity, Superoleophobicity, and Superaerophobicity.
29 *ChemNanoMat* **2019**, *5*, 241-249.
- 30 33. Feng, X. Q.; Gao, X. F.; Wu, Z. N.; Jiang, L.; Zheng, Q. S., Superior Water Repellency
31 of Water Strider Legs with Hierarchical Structures: Experiments and Analysis. *Langmuir* **2007**,
32 *23*, 4892-4896.
- 33 34. Hu, D. L.; Chan, B.; Bush, J. W. M., The Hydrodynamics of Water Strider Locomotion.
34 *Nature* **2003**, *424*, 663-666.
- 35 35. Hu, D. L.; Bush, J. W. M., Meniscus-Climbing Insects. *Nature* **2005**, *437*, 733-736.
- 36
37
38
39
40
41
42
43
44

45 Toc

